Kossel Effect in Periodic Multilayers

Karine Le Guen, Jean-Michel André, Meiyi Wu, Vita Ilakovac, Franck
Delmotte, Sébatien de Rossi, Françoise Bridou, Evgueni Meltchakov, Angelo
Giglia, Stefano Nannarone, et al.

Kossel Effect in Periodic Multilayers

Karine Le Guen[1,*], Jean-Michel André[1], Meiyi Wu[1], Vita Ilakovac[1,2], Franck Delmotte[3],
Sébatien de Rossi[3], Françoise Bridou[3], Evgueni Meltchakov[3], Angelo Giglia[4],
Stefano Nannarone[4], Zhanshan Wang[5], Qiushi Huang[5], Zhong Zhang[5],
Jingtao Zhu[5], Yuchun Tu[6], Yanyan Yuan[7], Ian Vickridge[8], Didier Schmaus[8,9], Emrick Briand[8],
Sébastien Steydli[8], Philippe Walter[10], and Philippe Jonnard[1]

[1] *Sorbonne Université, Faculté des Sciences et Ingénierie, UMR CNRS, Laboratoire de Chimie Physique – Matière et Rayonnement,
boîte courrier 1140, 4 place JussieuF-75252 Paris cedex 05, France*
[2] *Université de Cergy-Pontoise, Département de Physique, F-95031 Cergy-Pontoise, France*
[3] *Laboratoire Charles Fabry, Institut d'Optique GraduateSchool, CNRS, Université Paris-Saclay, 91127 Palaiseau Cedex, France*
[4] *CNR, Istituto Officina Materiali 34149 Trieste, Italy*
[5] *Key Laboratory of Advanced Micro-Structured Materials MOE, Institute of Precision Optical Engineering,
School of Physics Science and Engineering, Tongji University, Shanghai 200092, P. R. China*
[6] *Shanghai Institute of Laser Plasma, Shanghai 201800, P. R. China*
[7] *Jiangsu University of Science and Technology, School of Materials Science and Engineering, Mengxi Road 2, Zhenjiang,
Jiangsu Province, 212003, P. R. China*
[8] *Sorbonne Université, Faculté des Sciences et Ingénierie, UMR CNRS, Institut des NanoSciences de Paris, boîte courrier 840,
4 place Jussieu, F-75252 Paris cedex 05, France*
[9] *Université Paris Diderot-P7, F-75205 Paris cedex 13, France*
[10] *Sorbonne Université, Faculté des Sciences et Ingénierie, UMR CNRS, Laboratoire d'Archéologie Moléculaire et Structurale (LAMS),
boîte courrier 225, 4 place Jussieu, F-75005 Paris, France*

The Kossel effect is the diffraction by a periodically structured medium, of the characteristic X-ray
radiation emitted by the atoms of the medium. We show that multilayers designed for X-ray optics
applications are convenient periodic systems to use in order to produce the Kossel effect, modu-
lating the intensity emitted by the sample in a narrow angular range defined by the Bragg angle.
We also show that excitation can be done by using photons (X-rays), electrons or protons (or
charged particles), under near normal or grazing incident geometries, which makes the method
relatively easy to implement. The main constraint comes from the angular resolution necessary for
the detection of the emitted radiation. This leads to small solid angles of detection and long acqui-
sition times to collect data with sufficient statistical significance. Provided this difficulty is overcome,
the comparison or fit of the experimental Kossel curves, i.e., the angular distributions of the inten-
sity of an emitted radiation of one of the element of the periodic stack, with the simulated curves
enables getting information on the depth distribution of the elements throughout the multilayer. Thus
the same kind of information obtained from the more widespread method of X-ray standing wave
induced fluorescence used to characterize stacks of nanometer period, can be obtained using the
Kossel effect.

Keywords: Kossel Effect, X-ray Fluorescence, Multilayer, Bragg Diffraction, Interface.

1. INTRODUCTION

Following the dynamical theory of X-ray diffraction, a
characteristic X-ray emission generated from an atom
located inside a periodic medium can be diffracted by
the structure itself under Bragg conditions.[1] This emission
follows the ionization of a core level of an atom upon
irradiation by a beam of X-rays or charged particles and
is due to the spontaneous recombination of the electron
cloud. Interferences owing to the diffraction process cause
a modulation of the X-ray line intensity as a function of
the exit angle in the narrow angular range of the diffraction
pattern. This very first interpretation of X-ray diffraction

given in 1912 by M. von Laue, was established about twenty years later by Kossel using electron excitation of a crystal, leading to the observation of the so-called Kossel lines.[2]

Different ionizing radiations can be used to generate Kossel lines:[3]

—electrons from an electron gun,[4–7] a scanning electron microscope[8] or a transmission electron microscope;[9]

—X-ray photons from an X-ray tube,[10–12] a plasma source[13] or synchrotron radiation;[14–18] this case is analogous to the X-ray standing wave (XSW) technique[17, 19, 20] used to study the interfaces of multilayers[21] or X-ray waveguides[22] as well as thin surface films;[23]

—rapid charged particles (proton or ion beam) from an accelerator.[24–30]

In order to diffract X-rays the periodic medium can be a crystal[2, 31] or a multilayer made of a periodic alternation of two or more nanometer-thick thin films. In this paper we present examples of the study of periodic multilayers by using X-ray fluorescence induced by X-ray, electron or ion irradiation and modulated by the Kossel effect either. This process was used to obtain information on the interfacial roughness and interdiffusion in multilayers dedicated to X-ray optics.[10] In this case, Kossel diffraction can be viewed as the reverse of XSW[14, 19, 32] at grazing exit[33] and in multilayers.[34] Comparison between grazing incidence and grazing exit fluorescence can be found in Refs. [35–39] and their theory in Refs. [40, 41]. However, in grazing exit mode, these techniques are applied to quantify impurities at the top of the structure or in shallow dopants.[42] Applied to multilayers, XSW is only used in the grazing incidence mode,[33, 40] generally to probe thin layers deposited on the top of the multilayer[34, 43] or to probe the interfaces of the multilayer itself.[44] Indeed, the standing wave generated by the characteristic emission has the same period as the multilayer. Then, by rotating the sample in an angular range centered on the Bragg angle, defined by the multilayer period and the wavelength of the emitted radiation, it is possible to move the nodes and anti-nodes of the electric field to particular locations within the stack, for example to an interface or to the centre of a layer, and thus to locate the origin of the generated X-ray signal with great depth sensitivity.[34] Thus, the Kossel effect combined to X-ray fluorescence of characteristic X-rays is helpful to determine the structural parameters (thickness, roughness and composition of the layers and interlayers if any) of a periodic stack. It is a complementary tool to more widely used techniques such as X-ray fluorescence and photoelectron spectroscopies employed without angular variation, X-ray reflectivity, transmission electron microscopy.

This paper, which illustrates the Kossel effect in multilayers through examples of studies performed by the authors, is organized as follows. As far as the Bragg law ($p\lambda = 2d\sin\theta$, where λ is the wavelength of the diffracted radiation, p the diffraction order, d the period of the diffracting medium and θ the glancing angle of the

radiation) is concerned, we focus the experimental section on the geometrical details. The specific details regarding the presented experiments can be founded in the annexes at the end of the paper. We then explain how the angular distribution of the fluorescence intensity can be calculated. We take into account both the generation of the ionizations inside the stack and the depth distribution of the electric field of the emitted radiation. In the results section, we present examples of studies performed under X-ray, electron and proton irradiation.

2. GEOMETRY OF KOSSEL EXPERIMENTS

Since the experimental arrangement depends a lot on which kind of apparatus is used for the Kossel experiment, we only give brief comments on the different possibilities here. When characteristic emission is generated upon X-ray irradiation, a laboratory plasma source or X-ray tube working in the hard X-ray range or a synchrotron beamline working in the soft or hard X-ray range can be used, with the synchrotron offering a larger choice of experimental conditions due to the high brightness. For example, using long wavelength in the soft X-ray range makes it possible to work away from extreme grazing take-off angles, which could lead to alignment difficulties. When using electron irradiation an electron gun can be used provided it accelerates electrons up to a sufficiently high energy to create the core hole ionizations necessary for the characteristic emission generation. The ionization with a particle beam requires a dedicated facility in order to produce ions having an energy of the order of the MeV, leading to high ionization cross sections. There are many of these accelerators around the world.

We show on Figure 1(a) a schematic view of the configuration of Kossel experiments, where there is 60° between the incident and detected beams. However, most often, the detection of the characteristic photons is fixed and takes place in a direction at right angle with respect to the incident beam (photons, electrons or ions), which is also generally fixed. Thus, the experiment is made by rotating the sample. However, one can imagine Kossel experiments with a fixed sample and a rotating detector. The take-off (or detection) angle is tuned in the range of the Bragg angle related to the multilayer period and the emitted energy. The detection is made with an energy dispersive spectrometer. A spectrum is acquired for each of the scanned take-off angles. Then the measured intensity under a peak characteristic of an element, after background subtraction, is plotted as a function of the take-off angle. This so-called Kossel curve exhibits an intensity modulation centered at the Bragg angle. The treatment of the spectra can be more or less difficult depending on the possible interferences between spectral lines and on the intensity of the Bremsstrahlung. For example, it could be possible to switch from L to K lines to avoid interferences or to be able to neglect the background upon proton excitation.
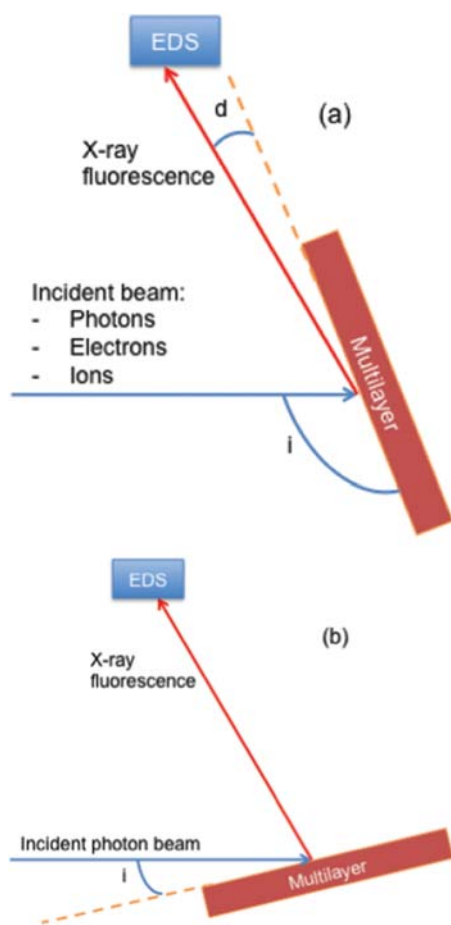
Figure 1. (a) Configuration for a Kossel experiment showing the incident and detected fluorescence beams and the multilayer sample. In this particular case there is 60° between the direction of the incident and the one of the detected characteristic photons. The take-off or detection angle is noted "*d*" and varied in the range of the Bragg angle related to the multilayer period and emitted energy. The incident beam is fixed and the experiment is carried out by rotating either the sample if the detector is fixed, or the detector if the sample is fixed. (b) Configuration for a standard standing wave experiment. The glancing angle of the photons is noted "*i*" and varied in the range of the Bragg angle related to the multilayer period and incident photon energy.

We show on Figure 1(b) the configuration of a standard XSW experiment. The glancing angle of the photons is tuned in the range of the Bragg angle related to the multilayer period and the incident photon energy. It is not possible to use electrons or ions as incident particles because their associated wavelength is much too small with respect to multilayer of nanometer period. The fluorescence intensity is measured as a function of the glancing angle. In this case, the angular resolution is given by the divergence of the incident beam, which can be made very small with X-ray irradiation thanks to collimation optics used with X-ray tube or on synchrotron beamlines. The detector can be placed very close to the sample leading to a large solid

angle of detection and a high collected intensity. For Kossel experiments, the angular resolution is governed by the aperture of the detector, which has to be placed far away from the sample or collimated with a slit, in order to observe Kossel features. Thus, the collected intensity is low and the acquisition time can be long (a few hours). However the configuration for the incident beam is more flexible than in classic standing wave experiments. This could be useful for example to decrease the imprint of the incident beam on the surface and thus obtain a lateral resolution on non-homogeneous samples. Kossel experiments are also interesting when photon irradiation is not available.

3. THEORY AND SIMULATION DETAILS

3.1. Simulation of the Detected Fluorescence Radiation

Two main methods may be used to calculate the intensity and spatial distribution of the fluorescence emission under the Kossel condition: (a) the direct method where the fluorescence is considered as an electromagnetic (X-ray) emission from an oscillating dipole excited by a primary beam of particles such as photons, electrons or protons, and whose depth distribution (in energy and space) is calculated by an appropriate code (see following sub-section), the emission of the dipole in the periodic multilayer being treated by a specific method; (b) the indirect method based on the application of a reciprocity principle. From the historical point of view, the indirect method was the first one implemented to interpret the Kossel structure by von Laue[2, 45] and is that mainly used until now to simulate the Kossel effect in periodic multilayers.[11] Both methods, direct and indirect, require the determination of the in-depth distribution in space and in energy of the exciting radiation since the intensity of the emitted fluorescence depends on the strength of the excitation of the emitting atoms. Let us describe in further details these two approaches.

(a) *Direct method*. The problem is reduced to the calculation of the electric field radiated in far field by an oscillating dipole embedded in a periodic multilayer. This problem is generally treated by the Green method. The main drawback of the method is that it leads to computational difficulties: in the spatial domain, Green's functions are represented by Sommerfeld integrals with an oscillatory nature[46] and in the spectral domain they are obtained as closed-form expressions with slow-decaying nature. An alternative way is to solve the propagation equation with a source term (inhomogeneous differential equation, IDE) corresponding to the oscillating dipole. The solution of this equation is obtained as the sum of the general solution of the homogeneous equation and of a particular solution of the IDE and by applying the appropriate boundary conditions. The propagation of the total field is performed by means of a matrix formalism inspired

from Abelès' work. The calculation of the far field is achieved without difficulty by computing an integral by the saddle-point method.[7] This approach has been developed by André et al.[47] in the context of the standing-wave enhanced fluorescence.

(b) *Indirect method*. This is based on the use of the Lorentz reciprocity theorem (in its Rayleigh-Carson form), which states that the relationship between an oscillating source and the corresponding radiated field is unchanged if one exchanges the location where the source is placed and that where the field is detected. In practice the calculation is reduced to the determination of the field at each point of multilayer by a standard method such as the Abelès matrix or the Parratt recursive methods.[48] Theoretical details on the Chauvineau recursive method[10] based on the calculation of optical thin films properties[49] can be found in Ref. [50]. It is an interesting approach from the theoretical point of view but the computation may be time-consuming for large multilayer structures since a good accuracy requires a sampling with small thickness steps within the multilayer structure, especially when one takes into account interfacial roughness. Let us outline that since the use of the reciprocity principle initiated by M. von Laue to interpret Kossel effect, this indirect method is nevertheless the preferred one.

3.2. Simulation of the Exciting Primary Radiation

The calculation of the depth distribution of the exciting radiation depends considerably on the nature of the radiation. For photons, the incident energy has a constant value but secondary photons of lower energy can be created during the interaction with the matter of the multilayer by fluorescence or inelastic (Raman) scattering. Nevertheless the yield of these processes is relatively small and these "secondary" photons are generally neglected. Thus, from the Bragg condition, a Beer-Lambert law is sufficient to describe the beam attenuation. For electrons, the distribution in energy is a more complicated problem since they can undergo many inelastic and elastic collisions, so that it is necessary to call upon detailed description of their individual trajectories. However, owing to the well-developed electron microprobe analysis field, there exist many codes, Monte-Carlo or semi-empirical, to calculate the depth distribution of the ionizations within a solid. The energy (and therefore the ionisation cross section) of protons of several MeV, such as those delivered by electrostatic accelerators, can be considered constant within the multilayer thickness which is in order of few hundreds of nanometers.

4. RESULTS AND DISCUSSION

4.1. Photon Excitation

We present an example of Kossel curves obtained upon photon excitation.[17] Experiments took place at the BEAR beamline of the Elettra synchrotron working in the soft X-ray range. The multilayers, prepared by magnetron sputtering, were periodic tri-layers: Mg/Co/Zr and Mg/Zr/Co and correspond respectively to the following stacks, going from the Si substrate to the superficial capping layer:

• Si/[Mg (5.45 nm)/Co (2.45 nm)/Zr (1.50 nm)]×30/B$_4$C (3.50 nm);

• Si/[Mg (5.45 nm)/Zr (1.50 nm)/Co (2.45 nm)]×30/B$_4$C (3.50 nm).

They only change by their deposition order. The indicated thicknesses are those aimed for during the preparation. The incident photon energies used to generate the Co Lα and Mg Kα emissions were 807.6 and 1332 eV respectively. More experimental details can be found in Ref. [17].

We present the Kossel curves obtained on these samples in Figure 2, displaying the intensity of the characteristic emissions as a function of the take-off angle. On all curves, above an increasing background, features occur as
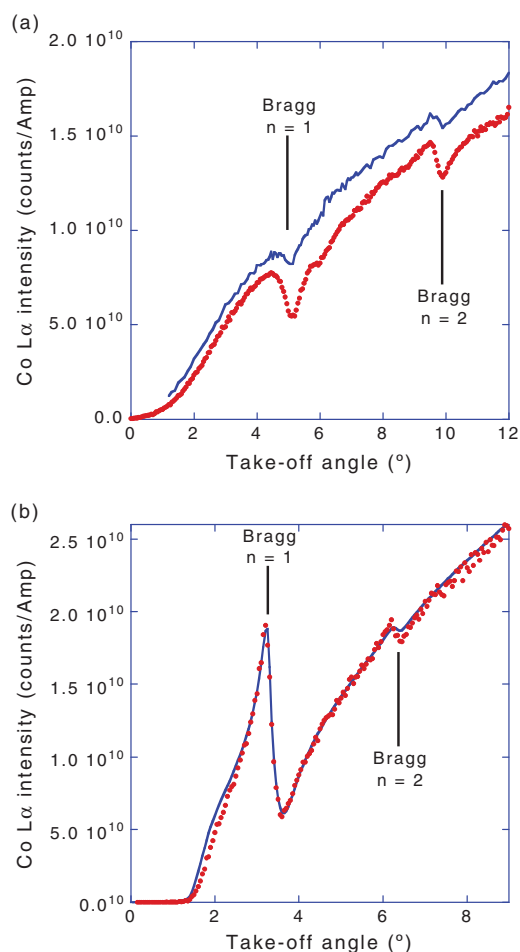

Figure 2. Kossel curves of the Mg/Zr/Co (line) and Mg/Co/Zr (dots) multilayers obtained from the Co Lα (a) and Mg Kα (b) characteristic emissions. The vertical bars indicate the position of the Bragg angle at the first and second diffraction orders.

expected at the Bragg angles, calculated from the energy of the emissions and the multilayer period at the first and second diffraction orders. These features appear at lower angles for the Mg Kα emission, owing to its higher energy (1253 eV) with respect to the Co Lα emission (776 eV). When comparing both samples, we observe that Mg/Zr/Co leads to less contrasted curves with respect to Mg/Co/Zr, particularly for the Co Lα emission.

We know from previous studies that Zr-on-Co interfaces (present in the Mg/Co/Zr stack) are abrupt, whereas the Co-on-Zr interfaces (present in the Mg/Zr/Co stack) are diffuse enough so that it is possible to consider the two Co and Zr layers as a single mixed layer. This was deduced from nuclear magnetic resonance and X-ray emission spectroscopies giving the chemical states of the Co and Mg atoms, respectively.[51–53] Using these results and the indirect method,[10,49] we simulate and fit the Kossel curves of Mg/Co/Zr considered as a tri-layer system, while for the Mg/Zr/Co system it is necessary to model a Mg/Co$_x$Zr$_y$ bilayer system with $x/y = 3.5$. This is illustrated in Figure 3 for the Co Lα emission of Mg/Zr/Co. Let us note that, even if the fit with the bi-layer structure is better than the one with the tri-layer system, the agreement between simulation and experiment is not perfect. This is due to the fact that the emission energy of the Co Lα emission ($3d$–$2p_{3/2}$ transition), 776 eV, is very close to the Co $2p_{3/2}$ ionization threshold, 778 eV. In other words, in this spectral range the Co optical constants are not known with high accuracy since they are strongly varying, and in addition they critically depend on the chemical state of the cobalt atoms.

Let us note that this problem does not occur for the Mg Kα emission ($2p$–$1s$ transition) since its energy, 1254 eV, is far from the Mg $1s$ ionization threshold at 1303 eV.[54] In this case, the simulations reproduce fairly the experimental Kossel curves and are in full agreement with the values of thicknesses and roughnesses deduced from the reflectivity measurements or from standard XSW experiments.
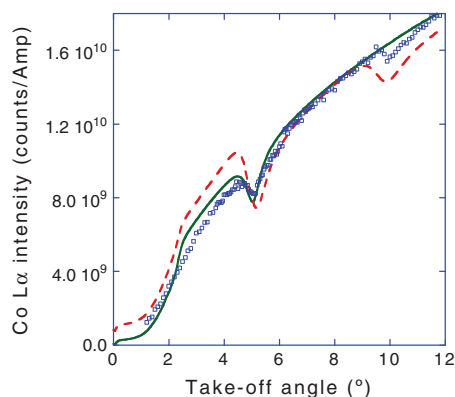
4.2. Electron Excitation

We now present an example of a Kossel curve obtained with a laboratory apparatus equipped with an electron gun to generate the characteristic emissions.[6] In this case, we consider the following multilayer prepared by triode DC sputtering and designed with the following structure: Si substrate/[W (1 nm)/C (2 nm)]×30. We look to the intensity of the W Mα emission (1775 eV; $4f$–$3d_{5/2}$ transition) excited by 4 keV electrons. The resulting Kossel curve is presented on Figure 4 compared to the simulated intensity. The simulation is convolved by a rectangular function representing the 0.2° angular aperture of the detector and also takes into account the depth distribution of the W $3d_{5/2}$ ionizations. This distribution is calculated from a semi-empirical model[55] describing the generation of the ionizations within a solid under electron irradiation: they take place over the whole thickness of the stack but most of them occur in the first 15 bi-layers of the stack. This is mainly conditioned by the path of the electrons through the stack.

The simulation[10,49] is in good agreement regarding the position (inflexion point) of the Kossel feature but only reproduces qualitatively the shape of the curve. This discrepancy in the intensity variation of the background could be ascribed to a non-optimized description of the in-depth ionizations. Indeed, for this purpose we used a semi-empirical model[55] with the periodic stack replaced by a thick film having the thickness and mean composition of the multilayer.

4.3. Proton Excitation

We present an example of Kossel curve obtained upon proton irradiation produced by a Van de Graff accelerator.[56] The multilayer structure is Si substrate/[Sc (0.92 nm)/B$_4$C (0.20 nm)/Cr (0.60 nm)]×100. The indicated thicknesses are those deduced from X-ray reflectivity measurements.

Figure 3. Co Lα Kossel curve of the Mg/Zr/Co multilayer (dots) and its fit with a tri-layer model (dashed line) and a bi-layer model (solid line).
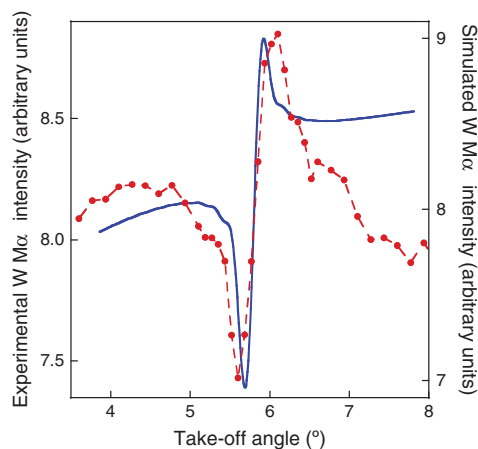

Figure 4. W Mα Kossel curve of the W/C multilayer excited by 4 keV electrons: dots and dashed line, experiment; solid line, simulation.

The sample was prepared by magnetron sputtering.[57] A thin B_4C capping layer was put on top of the stack to prevent oxidation. The proton energy was set to 2.0 MeV to insure high ionization cross sections, leading to the detection of the Cr Kα (4090 eV) and Sc Kα (5414 eV) lines. In this condition, the depth distribution of the ionizations within the whole stack is uniform. The simulations for protons were performed using the same code using the indirect method as the one developed for photons, setting the optical indices of the incident radiation to the constant values of 1 and 0 for the real and imaginary parts, respectively. The incident beam is not affected by refraction nor absorption, ensuring a uniform distribution of the ionizations with the depth.

We show in Figures 5(a) and (b) the Kossel curves corresponding to the Cr and Sc Kα emissions. They are obtained by making a scan of sample holder while measuring the emitted spectrum with a silicon drift detector (SDD). The angular scale offset has been calibrated by using the position of the total internal reflection obtained from a large scan (not shown) starting from the zero angle. Owing to the poor counting statistics, despite a total acquisition time of about 2 days, the experimental curves are quite noisy and poorly contrasted. The total dose on the sample is 150 or 120 μC times the number of points in the angular scan. The intensity modulations, a dip followed by a peak for Cr and the reverse for Sc, are well observed at the correct position. The simulations[10, 49] have been broadened by a 0.1° wide rectangular function representing the aperture of the detector. They reproduce the general shape of the curves (position, background) but not their contrast owing to the poor counting statistics.

To overcome the limitation of long counting times in Kossel experiments, we suggest using energy-dispersive CCD cameras[58] whose individual pixels each acquire an X-ray spectrum. Laboratory demonstration of this way of working has been given recently[13, 59] and we show our preliminary result with such a device in Figures 5(c) and (d). This significantly reduces the scanning time as the whole relevant angular range could be measured at once. Moreover, owing to the small size of the CCD pixels, some tens of micrometers, compared to the width of the slits generally used for Kossel experiment, some hundreds of micrometers, it would be possible to place the detector
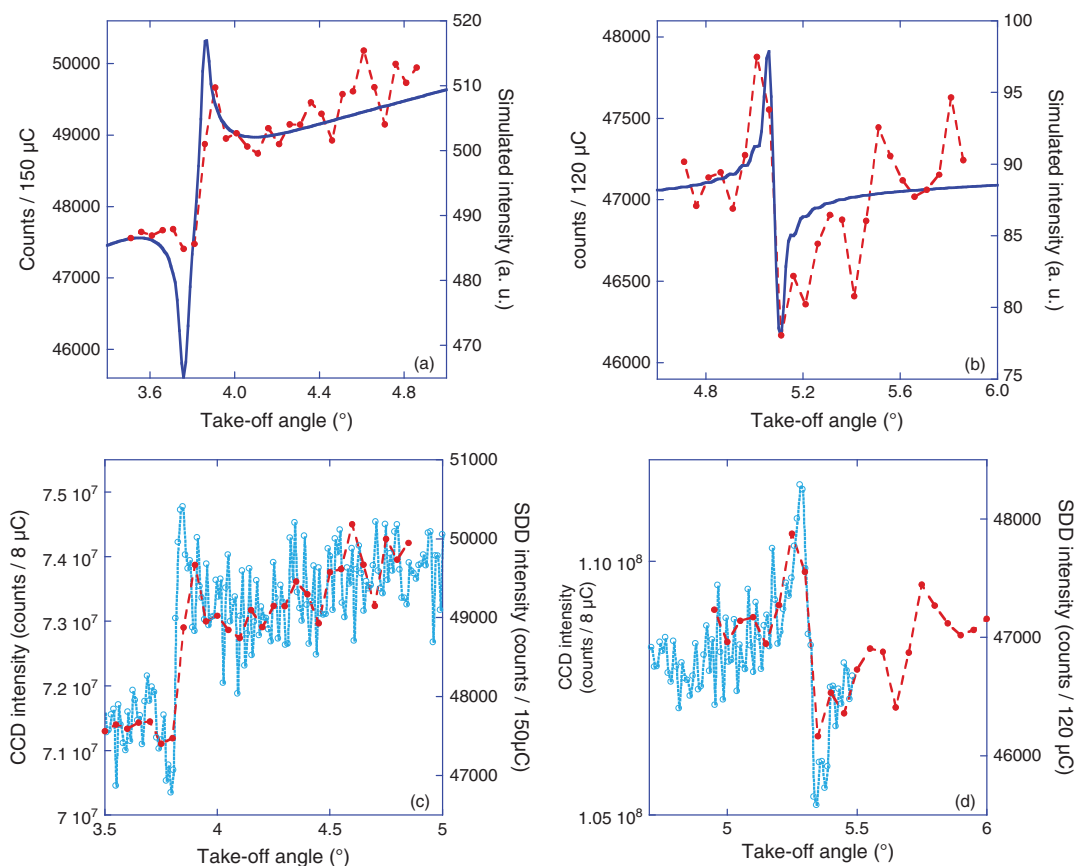

Figure 5. Cr Kα (a, c) and Sc Kα (b, d) Kossel curves of the Cr/B_4C/Sc multilayer excited by 2.0 MeV protons: (a) and (b) Present the comparison between the experiment with SDD (dots and dashed line) and the simulation (solid line); (c) and (d) present the comparison of the experimental curves obtained with SDD (red dots and line) and CCD (blue dots and line).

closer to the sample and thus increase the solid angle of detection and improve the counting statistics.

The Cr and Sc Kα Kossel curves obtained with the energy-dispersive CCD camera are shown in Figures 5(c) and (d) in comparison to the ones obtained with the SDD. In this case the acquisition time has been decreased to only 200 s and the total dose on the sample was limited to 8 μC. The counting statistics is not yet very good with such an acquisition time but would have been satisfactory with one hour. Anyway, despite these not optimal conditions, the improvement with respect to the SDD is clear as a better angular resolution (≈0.05° between the position of minium and maximum with the CCD and ≈0.15° with the SDD) and a better contrast (relative intensity of the minimum and maximum of the curve with respect to the background intensity) of the Kossel feature can be observed.

5. CONCLUSION

It is now possible to obtain the Kossel curves from periodic structures, crystal or multilayers, with any kind of ionization radiation, X-rays, electrons or ions. There is no strict requirement on the direction of the incident beam on the sample. For example, the near-normal incidence can be chosen in order to minimize the imprint of the incident beam and thus enabling to map inhomogeneous samples. There is also no strict requirement on the monochromaticity of the incident beam. It is enough that the incident energy is larger than the binding energy of the core level involved in the observed characteristic emission.

Owing to the required small aperture of the detector in order to get a sufficient angular resolution, the collected intensities of the characteristic emissions are small despite large counting times. This is mainly problematic for electrons and ion irradiation. The high flux available in modern synchrotrons enables measuring spectra with a reliable statistics and thus making accurate comparison with simulations. In this case, the Kossel curve can be used to describe a multilayer stack and especially get insight on the interface composition. The advantage of using incident charged particles is the possibility to obtain well focused beams and so to probe not only the depth of a sample but also its surface, with a spatial resolution down to a few tens of nanometers. The versatility and wide availability of electron guns makes electron irradiation an interesting option. Beams of rapid positive charged particles are also quite attractive because on the facilities delivering such beams it is possible to benefit complementary techniques such as Rutheford backscattering spectrometry or nuclear reaction analysis. When using X-rays as incident particles, the technique is photon-in photon-out, so insulating samples (presence of a silica substrate or dielectric layers for example) can be analysed without suffering from charging effect. Let us note, that the multilayers designed for the X-ray range have generally a total thickness of a few hundreds of nm and so electrons or photons of a few keV or

protons of a few MeV penetrate the whole structure. Thus the maximal depth of information is the thickness of the stack for the three excitation cases. Let us also note that the magnitude of the ionization cross sections are of the same order of magnitude (10^3–10^5 barns, depending on the involved electron orbital and atomic number) for electrons or photons of a few keV or protons of a few MeV. So the number of generated characteristic photons mainly depends on the number of incident particles: ≈10^{13} electrons or protons per second for an electron or proton beam of a few μA; ≈10^{13} photons per second for third generation synchrotron.

Let us note that Kossel lines have also been observed in a crystal with thermal neutrons.[60] Indeed, X-rays and thermal neutrons have wavelengths of the same order of magnitude and so can be subject to the same kind of diffraction process. The possibility to make inside source holography was already proposed by the authors.[60] We could consider using periodic multilayers to also obtain Kossel lines with such neutrons.

Finally, let us note that the enhancement in the Bragg direction of characteristic X-ray emissions generated within a crystal is interesting for the development of X-ray sources. The basic idea is to use the phase-matched regime which takes place in the Bragg diffraction to realize a distributed-feedback laser,[61] similar to the ones developed in the visible or IR ranges.[62] Indeed, the periodic structure of the crystal or multilayer provides feedback by Bragg coupling between the forward- and backward-travelling waves while the periodic structure behaves as a spatially distributed resonator. Thus an X-ray laser could be envisaged, the optical cavity and the active medium being the periodic multilayer and an incident free electron laser beam generating the inversion of population.

APPENDIX

We give here more details about the apparatus and acquisition conditions used in the results section.

Photon Excitation

The experiments were performed with *s*-polarized incident primary radiation on the BEAR beamline of the Elettra synchrotron facility, where the angle between the incident and detection directions is fixed and equal to about 60° owing to mechanical constraints. To get a good angular resolution the detector was moved 300 mm away from the sample resulting in a low collected intensity. However, this was partly compensated for by using a large divergent incident beam, thus increasing the incident flux. The detection of the fluorescence radiation was done by using a silicon drift detector (SDD) cooled to around −15 °C.

Taking into account the aperture of the SDD, 5 mm, and its distance to the sample leads to a 0.9° angular aperture. To improve the angular resolution, a 0.5 mm wide slit is

placed at 140 mm from the sample and 160 mm from the SDD. This leads to an angular acceptance of 0.2°.

Electron Excitation

The tungsten atoms are ionized by an electron beam produced from a Pierce gun (0–10 keV, 0–10 mA). The irradiated surface is about 1 cm^2, leading to a current density of a few tenths of mA/cm^2. The measurements are performed for 4.0 keV incident electron energies.

The experimental setup is such that the directions of the incident electrons and the detected photons are perpendicular. The rotation axis of the sample holder is perpendicular to the plane defined by the electron and photon directions. This device enables the variation of the angle between the sample surface and the direction of the detected photons.

The tungsten characteristic emission is analyzed with a high-resolution Johann-type X-ray spectrometer, using an InSb (111) crystal ($d = 0.374$ nm) at the first reflection order. The spectrometer is positioned at the maximum of the tungsten emission. Because of the finite height of the irradiation area on the multilayer, about 1 cm, and the acceptance angle of the spectrometer, there is about 0.2° between the detection angles measured at the ends of the multilayer. This angular spread leads to an instrumental broadening. A misorientation of the sample during the rotation could lead to an extra instrumental broadening.

Proton Excitation

Protons of 2.0 MeV produced by the Van de Graaff accelerator of the SAFIR Platform of Sorbonne Université were used to excite the sample. With such energy, the protons ionise the Sc and Cr atoms in their K shell uniformly over the full multilayer thickness. The size of the beam on the sample was approximately 2 mm and the beam current maintained between 100 and 150 nA for the duration of the experiments. The angle between the incident proton beam and the X-ray detector (SDD or CCD) was fixed at 90°. The distance between the sample and the detector was 115 mm. In addition to the beryllium window protecting the SDD from the atmosphere, a 60 μm thick Mylar film was placed in front of the detector to block the scattered protons. In the case of the CCD a 200 μm thick Be window was used.

A slit of ≈0.2 mm width was placed in front of the collimator of the SDD, giving an angular resolution of about 0.1°. The Kossel curve was obtained by scanning the rotation of the sample while measuring the intensity of the characteristic emissions. The acquisition time was long, about 2 days. So the proton beam was moved on the sample surface, from one pristine zone to another, so that the dose did not exceed 600 μC at a given location.

The energy-dispersive CCD camera is an iKon-M from Andor Technologies equipped with a 1024×1024 sensor array with 13×13 μm pixels. Instead of using the native spatial resolution, we select a 4×4 binning. Such selection

improves the energy resolution by minimizing the charge sharing effect between adjacent pixels while still providing adequate angular resolution. The camera spans an angular range of 2.7° and the angular acceptance of 0.025° for the 4×4 binned pixels. In this case, it was possible to obtain a Kossel curve in a few hundreds seconds.

References and Notes

1. R. W. James, The Optical Principle of the Diffraction of X-rays, Sir Lawrence Bragg, London (**1962**), at https://archive.org/details/opticalprinciple031059mbp.
2. A. Authier, *Z. Für Krist.* 227, 36 (**2012**).
3. E. Langer and S. Däbritz, *IOP Conf. Ser.: Mater. Sci. Eng.* 7, 012015 (**2010**).
4. V. V. Lider, *Crystallogr. Rep.* 56, 169 (**2011**).
5. P. Jonnard, J.-M. Andreì, C. Bonnelle, F. Bridou, and B. Pardo, *Appl. Phys. Lett.* 81, 1524 (**2002**).
6. P. Jonnard, J.-M. André, C. Bonnelle, F. Bridou, and B. Pardo, *Phys. Rev. A* 68, 032505 (**2003**).
7. J.-M. André, P. Jonnard, and B. Pardo, *Phys. Rev. A* 70, 012503 (**2004**).
8. E. Langer, Ph.D. Thesis, Der Einfluß von Kristallfehlern auf Kossel und Weitwinkel Interferenzen (**2004**), at www.qucosa.de/fileadmin/data/qucosa/documents/1346/1122972592603-3817.pdf.
9. J. Taftø and J. C. H. Spence, *Science* 218, 49 (**1982**).
10. J.-P. Chauvineau and F. Bridou, *J. Phys. IV* 06, C7-53 (**1996**).
11. J.-P. Chauvineau, O. Hainaut, and F. Bridou, *J. Phys. IV* 06, C4-773 (**1996**).
12. M. A. Chuev, M. V. Koval'chuk, V. V. Kvardakov, P. G. Medvedev, E. M. Pashaev, I. A. Subbotin, and S. N. Yakunin, *JETP Lett.* 91, 191 (**2010**).
13. J. Baumann, C. Herzog, M. Spanier, D. Grötzsch, L. Lühl, K. Witte, A. Jonas, S. Günther, F. Förste, R. Hartmann, M. Huth, D. Kalok, D. Steigenhöfer, M. Krämer, T. Holz, R. Dietsch, L. Strüder, B. Kanngießer, and I. Mantouvalou, *Anal. Chem.* 89, 1965 (**2017**).
14. S. Marchesini, M. Belakhovsky, A. Q. R. Baron, G. Faigel, M. Tegze, and P. Kamp, *Solid State Commun.* 105, 685 (**1998**).
15. C. Schetelich, S. Brenner, and V. Geist, *J. Synchrotron Radiat.* 5, 102 (**1998**).
16. P. Jonnard, Y.-Y. Yuan, K. Le Guen, J.-M. André, J.-T. Zhu, Z.-S. Wang, and F. Bridou, *J. Phys. B At. Mol. Opt. Phys.* 47, 165601 (**2014**).
17. Y. Tu, Y. Yuan, K. Le Guen, J.-M. André, J. Zhu, Z. Wang, F. Bridou, A. Giglia, and P. Jonnard, *J. Synchrotron Radiat.* 22, 1419 (**2015**).
18. G. Faigel, G. Bortel, and M. Tegze, *Sci. Rep.* 6, 22904 (**2016**).
19. T. Gog, D. Novikov, J. Falta, A. Hille, and G. Materlik, *J. Phys. IV* 04, C9-449 (**1994**).

20. J. Zegenhagen and A. Kazimirov, The X-ray Standing Technique: Principles and Applications, World Scientific Publishing Co. Pte. Ltd (**2013**).
21. S. Bera, D. K. Goswami, K. Bhattacharjee, B. N. Dev, G. Kuri, K. Nomoto, and K. Yamashita, *Nucl. Instrum. Methods Phys. Res. Sect. B Beam Interact. Mater. At.* 212, 530 (**2003**).
22. P. Rajput, A. Gupta, and D. K. Avasthi, *Nucl. Instrum. Methods Phys. Res. Sect. B Beam Interact. Mater. At.* 266, 1680 (**2008**).
23. A. Zargham, T. Schmidt, J. I. Flege, M. Sauerbrey, R. Hildebrand, S. Röhe, M. Bäumer, and J. Falta, *Nucl. Instrum. Methods Phys. Res. Sect. B Beam Interact. Mater. At.* 268, 325 (**2010**).
24. V. Geist and R. Flagmeyer, *Phys. Status Solidi A* 26, K1 (**1974**).
25. J. B. Roberto, B. W. Batterman, V. O. Kostroun, and B. R. Appleton, *J. Appl. Phys.* 46, 936 (**1975**).
26. V. Geist, R. Flagmeyer, D. Stephan, and H.-J. Ullrich, *Phys. Status Solidi A* 40, 113 (**1977**).
27. V. Geist, R. Flagmeyer, and G. Otto, *Phys. Lett. A* 64, 421 (**1978**).
28. V. Geist, C. H. Ehrlich, R. Flagmeyer, H. J. Ullrich, W. Greiner, and S. Rolle, *Cryst. Res. Technol.* 17, 245 (**1982**).
29. J. Rickards, *Nucl. Instrum. Methods Phys. Res. Sect. B Beam Interact. Mater. At.* 24, 621 (**1987**).
30. C. Schetelich, S. Weber, V. Geist, M. Schlaubitz, H. J. Ullrich, S. Kek, and H. G. Krane, *Nucl. Instrum. Methods Phys. Res. Sect. B Beam Interact. Mater. At.* 103, 236 (**1995**).
31. P. Pieranski, E. Dubois-Violette, F. Rothen, and L. Strzelecki, *J. Phys.* 42, 53 (**1981**).
32. T. Gog, D. Bahr, and G. Materlik, *Phys. Rev. B* 51, 6761 (**1995**).
33. O. Sakata and T. Jach, X-ray standing wave at grazing incidence and exit, The X-ray Standing Wave Technique, World Scientific Publishing Co. Pte. Ltd (**2013**), pp. 108–121.
34. M. J. Bedzyk and J. A. Libera, X-ray standing wave in multilayers, The X-ray Standing Wave Technique, World Scientific Publishing Co. Pte. Ltd (**2013**), pp. 122–131.
35. K. Tsuji, M. Huisman, Z. Spolnik, K. Wagatsuma, Y. Mori, R. E. Van Grieken, and R. D. Vis, *Spectrochim. Acta Part B At. Spectrosc.* 55, 1009 (**2000**).
36. K. Tsuji, *Spectrochim. Acta Part B At. Spectrosc.* 60, 1381 (**2005**).
37. P. Hönicke, Y. Kayser, B. Beckhoff, M. Müller, J.-C. Dousse, J. Hoszowska, and S. H. Nowak, *J. Anal. At. Spectrom.* 27, 1432 (**2012**).
38. J. Szlachetko and Y. Kayser, Techniques: RXES, HR-XAS, HEROS, GIXRF, and GEXRF, High-Resolution XAS/XES: Analyzing Electronic Structures of Catalysts, edited by J. Sa, CRC Press (**2015**), pp. 59–115, at https://www.crcpress.com/High-Resolution-XASXES-Analyzing-Electronic-Structures-of-Catalysts/Sa/p/book/9781138071575.
39. Y. Kayser, P. Hönicke, D. Banaś, J.-C. Dousse, J. Hoszowska, P. Jagodziński, A. Kubala-Kukuś, S. H. Nowak, and M. Pajek, *J. Anal. At. Spectrom.* 30, 1086 (**2015**).
40. D. K. G. de Boer, *Phys. Rev. B* 44, 498 (**1991**).
41. H. P. Urbach and P. K. de Bokx, *Phys. Rev. B* 63, 085408 (**2001**).
42. Y. Kayser, D. Banaś, W. Cao, J.-C. Dousse, J. Hoszowska, P. Jagodziński, M. Kavčič, A. Kubala-Kukuś, S. Nowak, M. Pajek, and J. Szlachetko, *X-ray Spectrom.* 41, 98 (**2012**).

43. S.-H. Yang, B. C. Sell, B. S. Mun, and C. S. Fadley, Probing multilayer nanostructures with photoelectron and X-ray emission spectroscopies excited by X-ray standing waves, The X-ray Standing Wave Technique, World Scientific Publishing Co. Pte. Ltd (**2013**), pp. 475–492.
44. F. Bridou, G. Cauchon, and M. Idir, *J. Phys. IV* 118, 137 (**2004**).
45. M. von Laue, *Ann. Phys.* 415, 705 (**1935**).
46. M. Paulus, P. Gay-Balmaz, and O. J. F. Martin, *Phys. Rev. E* 62, 5797 (**2000**).
47. J.-M. André, K. Le Guen, and P. Jonnard, *Spectrochim. Acta Part B At. Spectrosc.* 85, 55 (**2013**).
48. B. Pardo, T. Megademini, and J.-M. André, *Rev. Phys. Appliquée* 23, 1579 (**1988**).
49. P. H. Berning, Theory and calculations of optical thin films, Physics of Thin Films, G. Hass, NewYork, London (**1963**), pp. 69–122.
50. Y. Chambet, Ph.D. Thesis, Etude expérimentale de la diffusion des rayons x rasants par les multicouches pour optiques X-UV (**1993**), at http://www.theses.fr/1993PA112341.
51. K. Le Guen, M.-H. Hu, J.-M. André, P. Jonnard, S. K. Zhou, H. C. Li, J. T. Zhu, Z. S. Wang, N. Mahne, A. Giglia, and S. Nannarone, *Appl. Phys. A* 102, 69 (**2011**).
52. K. Le Guen, M.-H. Hu, J.-M. Andreì, S. K. Zhou, H. C. Li, J. T. Zhu, Z. S. Wang, C. Meny, A. Galtayries, and P. Jonnard, *Appl. Phys. Lett.* 98, 251909 (**2011**).
53. J. Zhu, S. Zhou, H. Li, Z. Wang, P. Jonnard, K. Le Guen, M.-H. Hu, J.-M. André, H. Zhou, and T. Huo, *Opt. Express* 19, 21849 (**2011**).
54. P. Jonnard and C. Bonnelle, *X-ray Spectrom.* 40, 12 (**2011**).
55. P.-F. Staub, P. Jonnard, F. Vergand, J. Thirion, and C. Bonnelle, *X-ray Spectrom.* 27, 58 (**1998**).
56. M. Wu, K. Le Guen, J.-M. André, V. Ilakovac, I. Vickridge, D. Schmaus, E. Briand, S. Steydli, C. Burcklen, F. Bridou, E. Meltchakov, S. de Rossi, F. Delmotte, and P. Jonnard, *Nucl. Instrum. Methods Phys. Res. Sect. B Beam Interact. Mater. At.* 386, 39 (**2016**).
57. C. Burcklen, Ph.D. Thesis, Microscope X dans la fenêtre de l'eau: Conception, miroirs à revêtements multicouches et métrologie associée (**2017**).
58. I. Ordavo, S. Ihle, V. Arkadiev, O. Scharf, H. Soltau, A. Bjeoumikhov, S. Bjeoumikhova, G. Buzanich, R. Gubzhokov, A. Günther, R. Hartmann, P. Holl, N. Kimmel, M. Kühbacher, M. Lang, N. Langhoff, A. Liebel, M. Radtke, U. Reinholz, H. Riesemeier, G. Schaller, F. Schopper, L. Strüder, C. Thamm, and R. Wedell, *Nucl. Instrum. Methods Phys. Res. Sect. Accel. Spectrometers Detect. Assoc. Equip.* 654, 250 (**2011**).
59. V. Szwedowski, J. Baumann, I. Mantouvalou, L. Bauer, W. Malzer, and B. Kanngießer, *Phys. Status Solidi C* 14, 1700158 (**2017**).
60. B. Sur, R. B. Rogge, R. P. Hammond, V. N. P. Anghel, and J. Katsaras, *Phys. Rev. Lett.* 88, 065505 (**2002**).
61. J.-M. André, K. Le Guen, and P. Jonnard, *Laser Phys.* 24, 085001 (**2014**).
62. H. Kogelnik and C. V. Shank, *J. Appl. Phys.* 43, 2327 (**1971**).